J|A|C|S
ARTICLES
Published on Web 12/27/2005

Crossover from Superexchange to Hopping as the Mechanism for Photoinduced Charge Transfer in DNA Hairpin Conjugates

Frederick D. Lewis,*,† Huihe Zhu,† Pierre Daublain,† Torsten Fiebig,*,‡ Milen Raytchev,‡ Qiang Wang,‡ and Vladimir Shafirovich*,§

Contribution from the Department of Chemistry, Northwestern University, Evanston, Illinois 60201, Department of Chemistry, Boston College, Chestnut Hill, Massachusetts 02467, and Department of Chemistry, New York University, New York, New York 10003

Received June 20, 2005; E-mail: lewis@chem.northwestern.edu; fiebig@bc.edu; vs5@nyu.edu

Abstract: The mechanism and dynamics of photoinduced charge separation and charge recombination have been investigated in synthetic DNA hairpins possessing donor and acceptor stilbenes separated by one to seven A:T base pairs. The application of femtosecond broadband pump−probe spectroscopy, nanosecond transient absorption spectroscopy, and picosecond fluorescence decay measurements permits detailed analysis of the formation and decay of the stilbene acceptor singlet state and of the charge-separated intermediates. When the donor and acceptor are separated by a single A:T base pair, charge separation occurs via a single-step superexchange mechanism. However, when the donor and acceptor are separated by two or more A:T base pairs, charge separation occurs via a multistep process consisting of hole injection, hole transport, and hole trapping. In such cases, hole arrival at the electron donor is slower than hole injection into the bridging A-tract. Rate constants for charge separation (hole arrival) and charge recombination are dependent upon the donor−acceptor distance; however, the rate constant for hole injection is independent of the donor−acceptor distance. The observation of crossover from a superexchange to a hopping mechanism provides a "missing link" in the analysis of DNA electron transfer and requires reevaluation of the existing literature for photoinduced electron transfer in DNA.

Introduction

The mechanism and dynamics of charge-transfer processes in DNA continue to attract the attention of both experimentalists and theoreticians.[1] We and others proposed that photoinduced charge transfer in systems possessing an excited acceptor separated from a guanine or deazaguanine donor by a small number of A:T base pairs occurs via a single-step superexchange process.[2−5] However, in the case of intercalated ethidium as the acceptor, multistep hopping followed by irreversible trapping was suggested as the mechanism for charge separation.[6] Theoretical analyses of DNA bridge-mediated electron transfer led to the proposal that photoinduced electron transfer might occur via either superexchange or hopping mechanisms, depending on the donor−bridge−acceptor energetics, endergonic bridge oxidation favoring a superexchange mechanism (Scheme 1a) and exergonic bridge oxidation favoring a hopping mechanism (Scheme 1b).[7] Because the superexchange process is expected to be strongly distance dependent and the hopping process weakly distance dependent, crossover from superexchange to hopping as the mechanism for charge separation in DNA is expected to occur at intermediate distances, as has been observed for charge separation in several donor−bridge−acceptor systems.[8−10] Following hole injection, hole transport can occur over both short and long distances in DNA.[11] Hole transport has been proposed to occur via a superexchange mechanism at short distances and via a hopping mechanism at

† Northwestern University.
‡ Boston College.
§ New York University.

(1) (a) Lewis, F. D. In *Electron Transfer in Chemistry*; Balzani, V., Ed.; Wiley-VCH: Weinheim, Germany, 2001; Vol. 3, pp 105−175. (b) Schuster, G. B., Ed. *Long-Range Charge Transfer in DNA, I and II*; Springer: New York, 2004; Vols. 236, 237. (c) Wagenknecht, H. A., Ed. *Charge Transfer in DNA*; Wiley-VCH: Weinheim, 2005.
(2) Lewis, F. D.; Wu, T.; Zhang, Y.; Letsinger, R. L.; Greenfield, S. R.; Wasielewski, M. R. *Science* **1997**, *277*, 673−676.
(3) Lewis, F. D.; Wu, T.; Liu, X.; Letsinger, R. L.; Greenfield, S. R.; Miller, S. E.; Wasielewski, M. R. *J. Am. Chem. Soc.* **2000**, *122*, 2889−2902.
(4) (a) Fukui, K.; Tanaka, T. *Angew. Chem., Int. Ed.* **1998**, *37*, 158−161. (b) Fukui, K.; Tanaka, K.; Fujitsuka, M.; Watanabe, A.; Ito, O. *J. Photochem. Photobiol., B: Biol.* **1999**, *50*, 18−27. (c) Hess, S.; Götz, M.; Davis, W. B.; Michel-Beyerle, M. E. *J. Am. Chem. Soc.* **2001**, *123*, 10046−10055. (d) Hess, S.; Davis, W. B.; Voityuk, A. A.; Rosch, N.; Michel-Beyerle, M. E.; Ernsting, N. P.; Kovalenko, S. A.; Lustres, J. L. P. *ChemPhysChem* **2002**, *3*, 452−455.
(5) Wan, C.; Fiebig, T.; Schiemann, O.; Barton, J. K.; Zewail, A. H. *Proc. Natl. Acad. Sci. U.S.A.* **2000**, *97*, 14052−14055.
(6) Wan, C.; Fiebig, T.; Kelley, S. O.; Treadway, C. R.; Barton, J. K.; Zewail, A. H. *Proc. Natl. Acad. Sci. U.S.A.* **1999**, *96*, 6014−6019.
(7) (a) Felts, A. K.; Pollard, W. T.; Friesner, R. A. *J. Phys. Chem.* **1995**, *99*, 2929−2940. (b) Jortner, J.; Bixon, M.; Langenbacher, T.; Michel-Beyerle, M. E. *Proc. Natl. Acad. Sci. U.S.A.* **1998**, *95*, 12759−12765.
(8) Abdel Malak, R.; Gao, Z.; Wishart, J. F.; Isied, S. S. *J. Am. Chem. Soc.* **2004**, *126*, 13888−13889.
(9) Paulson, B. P.; Miller, J. R.; Gan, W.-X.; Closs, G. *J. Am. Chem. Soc.* **2005**, *127*, 4860−4868.
(10) Weiss, E. A.; Tauber, M. J.; Kelley, R. F.; Ahrens, M. J.; Ratner, M. A.; Wasielewski, M. R. *J. Am. Chem. Soc.* **2005**, *127*, 11842−11850.
(11) (a) Giese, B.; Amaudrut, J.; Köhler, A.-K.; Spormann, M.; Wessely, S. *Nature* **2001**, *412*, 318−320. (b) Giese, B. *Acc. Chem. Res.* **2000**, *33*, 631−636. (c) Schuster, G. B. *Acc. Chem. Res.* **2000**, *33*, 253−260. (d) O'Neil, M. A.; Barton, J. K. *J. Am. Chem. Soc.* **2004**, *126*, 11471−11483. (e) Lewis, F. D.; Liu, J.; Zuo, X.; Hayes, R. T.; Wasielewski, M. R. *J. Am. Chem. Soc.* **2003**, *125*, 4850−4861.

Scheme 1. (a) Superexchange and (b) Hopping Mechanisms for Photoinduced Charge Separation between an Excited Acceptor and Ground-State Donor Separated by Three A:T Base Pairs

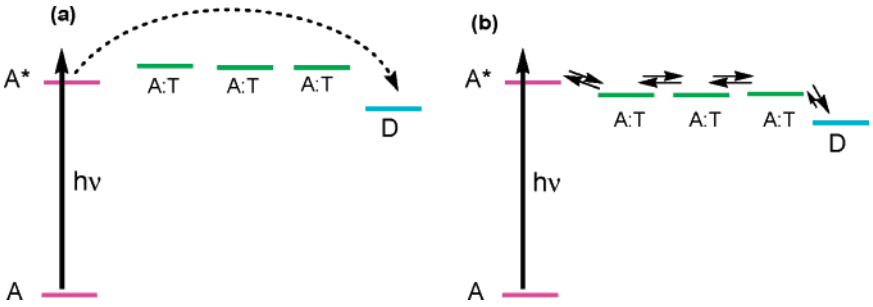

Chart 1. Structures of (a) Stilbene Linkers, (b) Donor−Acceptor Capped Hairpins, and (c) Stilbene-Linked Hairpins

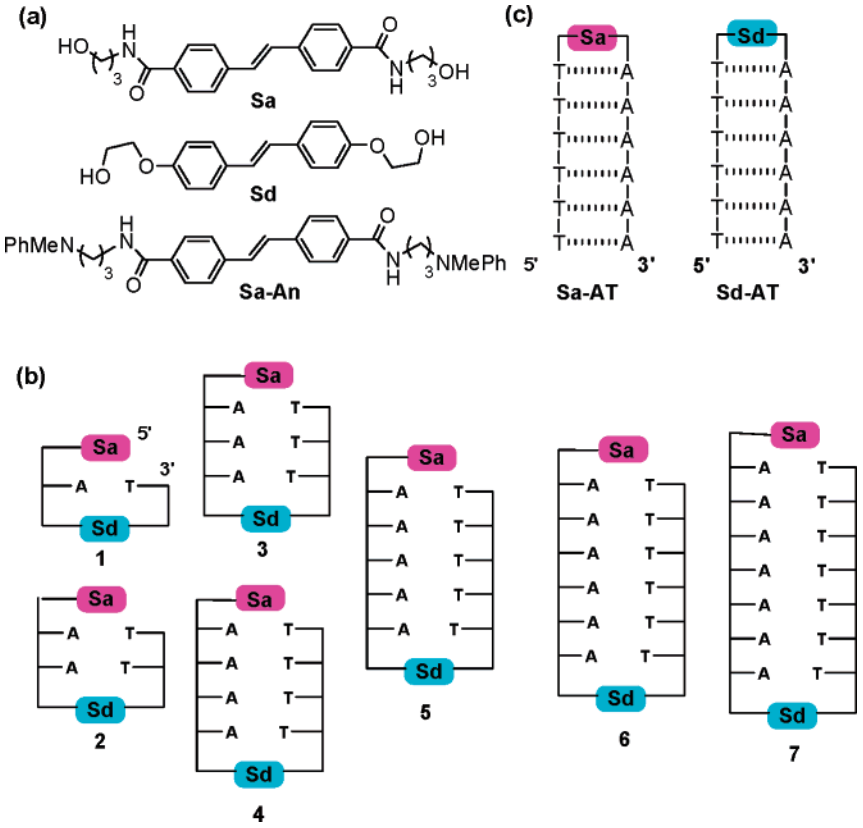

longer distances (alternatively viewed as polaron motion).[12] However, a crossover in mechanism has not been directly observed for photoinduced charge transfer in DNA.

We report here the results of our collaborative investigation of the dynamics and mechanism of charge separation and charge recombination in DNA hairpin conjugates possessing donor and acceptor stilbene chromophores (**Sa** and **Sd**, respectively, Chart 1a) separated by $(A:T)_n$ base pair domains (**1**−**7**, Chart 1b). The combination of femtosecond (fs) broadband pump−probe spectroscopy with an expanded spectral range,[13] nanosecond (ns) transient absorption,[14] and picosecond (ps) fluorescence decay measurements permits more detailed analysis of electron-transfer dynamics than was possible in previous studies in which **Sa*** serves as the electron acceptor and either guanine or **Sd** serves as the electron donor.[3,15] We have for the first time disentangled the various kinetic processes that are involved in photoinduced electron transfer in DNA: hole injection, hole arrival, and charge recombination. Furthermore, we have shown that each of these processes exhibits a characteristic distance dependence, resulting in the observation of a crossover from superexchange to interbase hopping as the mechanism for charge separation at a donor−acceptor plane-to-plane distance of ca. 10 Å (two base pairs) and at longer distances for charge recombination. Previous experimental studies of DNA charge separation and charge recombination dynamics can be analyzed in terms of these two limiting mechanisms.

(12) (a) Berlin, Y. A.; Burin, A. L.; Ratner, M. A. *J. Phys. Chem. A* **2000**, *104*, 443−445. (b) Berlin, Y. A.; Burin, A. L.; Ratner, M. A. *J. Am. Chem. Soc.* **2001**, *123*, 260−268. (c) Bixon, M.; Giese, B.; Wessely, S.; Langenbacher, T.; Michel-Beyerle, M. E.; Jortner, J. *Proc. Natl. Acad. Sci. U.S.A.* **1999**, *96*, 11713−11716. (d) Bixon, M.; Jortner, J. *Chem. Phys.* **2002**, *281*, 393−408. (e) Conwell, E. M.; Rakhmanova, S. V. *Proc. Natl. Acad. Sci. U.S.A.* **2000**, *97*, 4556−4560. (f) Conwell, E. M.; Park, J.-H.; Choi, H.-Y. *J. Phys. Chem. B* **2005**, *109*, 9760−9763.

(13) (a) Raytchev, M.; Mayer, E.; Amann, N.; Wagenknecht, H. A.; Fiebig, T. *Chem. Phys. Chem.* **2004**, *5*, 706−712. (b) Kaden, P.; Mayer-Enthart, E.; Trifonov, A.; Fiebig, T.; Wagenknecht, H.-A. *Angew. Chem., Int. Ed.* **2005**, *44*, 1636−1639.

(14) Shafirovich, V. Y.; Courtney, S. H.; Ya, N.; Geacintov, N. E. *J. Am. Chem. Soc.* **1995**, *117*, 4920−4929.

(15) Lewis, F. D.; Wu, Y.; Zhang, L.; Zuo, X.; Hayes, R. T.; Wasielewski, M. R. *J. Am. Chem. Soc.* **2004**, *126*, 8206−8215.

Experimental Section

Sample Preparation. Stilbene-4,4′-dicarboxylic acid was obtained from toluic acid by treatment with sulfur powder at high temperature.[16] The bis(3-hydroxypropyl)amide of stilbene-4,4′-dicarboxylic acid and the bis(2-hydroxyethyl)stilbene 4,4′-diether (**Sa** and **Sd**, respectively, in Chart 1a) were prepared and converted to their mono-DMT derivatives by reaction with 4,4′-dimethoxytrityl chloride.[17,18] The mono-DMT derivatives were reacted with 2-cyanoethyl diisopropyl-chlorophosphoramidite to afford the monoprotected, monoactivated diols. Hairpins **Sa-AT**, **Sd-AT**, and capped hairpins **1**−**7** (Chart 1) were prepared by means of conventional phosphoramidite chemistry using a Millipore Expedite oligonucleotide synthesizer. The conjugates were first isolated as trityl-on derivatives by reverse phase HPLC, and then detritylated in 80% acetic acid for 30 min. The presence of the stilbene linker was confirmed by absorption and fluorescence spectroscopy. Molecular weights were determined by using a Voyager DE-Pro MALDI-TOF mass spectrometer.

All samples were prepared in 0.1 M NaCl and 10 mM sodium phosphate, pH 7.2 (standard buffer). Hairpin concentrations were adjusted to provide absorbances of ca. 0.2 at the excitation wavelength for fluorescence measurements and ca. 0.3 for pump−probe measurements. Fluorescence quantum yields for **1**−**7** were determined using 355 nm excitation by comparing the fluorescence intensity at the emission maximum with that for **Sa-AT**.

Fluorescence Decay Measurements. In the picosecond single photon counting system, the sample is excited by a Coherent Mira 900 fs Ti:Sp laser that is pumped by an Innova 310 argon ion laser. The output of the Ti:Sp laser (700 nm) is passed through a Conoptics electrooptic light modulator system consisting of a model 350-160 Modulator, a model 25D Digital Amplifier, and a M305 Synchronous countdown device, to reduce the laser pulse frequency from 76 to 12 MHz, which is then doubled to provide excitation at 350 nm. Fluorescence emission is registered at 390 nm using an Aries FF250 monochromator. A Time Harp 100 PC card (PicoQuant, Germany) controlled by an IBM PC computer provides registration of the counts with rates of up to 80 MHz. After deconvolution (PicoQuant FluoFit software), the time resolution of this apparatus is ca. 35 ps. All experiments, including data collection and analysis, are controlled by an IBM PC computer using PicoQuant software.

Femtosecond Broadband Pump−Probe Spectroscopy. A detailed description of our experimental setup has been given elsewhere.[19] The pump wavelength was set to 355 nm for hairpins **1** and **2** and to 333 nm for hairpins **3** and **4**. The changes in optical density were probed by a femtosecond white-light continuum (WLC) generated by tight focusing of a small fraction of the output of a commercial Ti:Sp based pump laser (CPA-2010, Clark-MXR) into a 3 mm calcium fluoride (CaF_2) plate. The WLC provides a usable probe source between 300 and 750 nm. The WLC was split into two beams (probe and reference) and focused into the sample using reflective optics. After passing through the sample, both probe and reference beams were spectrally dispersed and simultaneously detected on a CCD sensor. The pump pulse (1 kHz, 400 nJ) was generated by frequency doubling of the compressed output of a home-built NOPA system (from 666 to 708 nm respectively, 7 μJ, 40 fs). To compensate for group velocity dispersion in the UV-pulse, an additional prism compressor was used. The overall time resolution of the setup is determined by the cross correlation function between pump and probe pulses, which is typically 120−150 fs (fwhm, assuming a Gaussian line shape). A spectral resolution of 7−10 nm was obtained. All measurements were performed with magic angle (54.7°) setting for the polarization of pump with respect to the polarization of the probe pulse. A sample cell with 1.25 mm fused silica windows and an optical path of 1 mm was used for all measurements. A wire stirrer was used to ensure fresh sample volume was continuously used during the measurement.

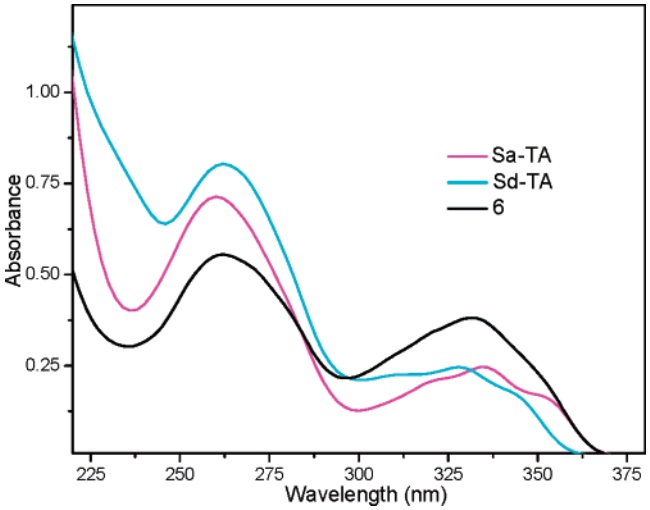

Figure 1. UV spectra of conjugates **Sa-AT**, **Sd-AT**, and **6** in aqueous buffer (0.1 M NaCl and 10 mM sodium phosphate, pH 7.2, concentrations of **Sa-AT** and **Sd-AT** adjusted to provide similar absorbance at 325 nm).

Nanosecond Transient Absorption Spectra. The transient absorption spectra and kinetics of the radical ions were monitored directly using a fully computerized kinetic spectrometer system (∼7 ns response time). The excitation source was a nanosecond Nd:YAG laser (Continuum Surelite II, ca. 6 ns pulse width, 10 Hz repetition rate, ∼10 mJ pulse^{-1} cm^{-2}, 355 nm excitation). The sample excitation frequency was reduced to 1 Hz by an electromechanical shutter and used to excite sample solutions (0.25 mL) of the oligonucleotides saturated with argon. The transient absorbance was probed along a 1 cm optical path by light from a pulsed 75 W xenon arc lamp with its light beam oriented perpendicular to the laser beam. The signal was recorded by a Tektronix TDS 5052 oscilloscope operating in its high-resolution mode. Satisfactory signal/noise ratios were obtained even after a single laser shot.

Results

Absorption and Fluorescence Spectra. The syntheses and characterization of the stilbene derivatives **Sa** and **Sd**, the dyad **Sa-An**, and the hairpins **Sa-AT** and **Sd-AT** (Chart 1a,c) have previously been described.[15,18,20] The capped hairpins **1**−**7** (Chart 1b) were prepared, purified, and characterized by methods employed for the preparation of capped hairpins with Sa linkers and capping groups.[15] Capped hairpins possessing one or more base pair are known to form folded structures that are stable at room temperature.[21,22]

The UV absorption spectra of **Sa**, **Sd**, **Sa-An**, **Sa-AT**, and **Sd-AT** have been reported.[3,23] The spectra of **Sa-AT**, **Sd-AT**, and **6** are shown in Figure 1. The 260 nm bands of all three conjugates are dominated by base pair absorption, and the long-wavelength bands are dominated by the stilbene absorption. The long-wavelength bands of **1**−**7** are superimposable. The **Sa-**

(16) Khalaf, A. I.; Pitt, A. R.; Scbie, M.; Suckling, C. J.; Urwin, J.; Waigh, R. D.; Young, S. C.; Fishleigh, R. V.; Fox, K. *Tetrahedron* **2000**, *56*, 5225−5239.
(17) Letsinger, R. L.; Wu, T. *J. Am. Chem. Soc.* **1995**, *117*, 7323−7328.
(18) Lewis, F. D.; Wu, Y.; Liu, X. *J. Am. Chem. Soc.* **2002**, *124*, 12165−12173.
(19) Raytchev, M.; Pandurski, E.; Buchvarov, I.; Modrakowski, C.; Fiebig, T. *J. Phys. Chem. A* **2003**, *107*, 4592−4600.
(20) Lewis, F. D.; Liu, X.; Wu, Y.; Miller, S. E.; Wasielewski, M. R.; Letsinger, R. L.; Sanishvili, R.; Joachimiak, A.; Tereshko, V.; Egli, M. *J. Am. Chem. Soc.* **1999**, *121*, 9905−9906.
(21) Lewis, F. D.; Liu, X.; Wu, Y.; Zuo, X. *J. Am. Chem. Soc.* **2003**, *125*, 12729−12731.
(22) Lewis, F. D.; Zhang, L.; Liu, X.; Zuo, X.; Tiede, D. M.; Long, H.; Schatz, G. S. *J. Am. Chem. Soc.* **2005**, *127*, 14445−14453.
(23) Lewis, F. D.; Wasielewski, M. R. In *Charge Transfer in DNA*; Wagenknecht, H.-A., Ed.; Wiley-VCH: Weinheim, Germany, 2005.

Table 1. Fluorescence Quantum Yields and Decay Data[a]

conjugate	Φ_f[b]	τ_1 (amp), ps[c]	τ_2 (amp), ns[c]	τ_3 (amp), ns[c]
Sa[d]	0.11	280, 362[f]		
Sd[e]	0.32	350, 379[f]		
Sa-AT	0.38[d]	45 (71)	0.86 (8)	2.2 (21)
1	<0.01			
2	0.033	38 (73)	1.7 (25)	*g*
3	0.15	66 (76)	0.37 (20)	1.4 (3)
4	0.26	40 (75)	0.58 (12)	1.4 (11)
5	0.29	81 (75)	1.24 (20)	2.0 (10)
6	0.31	95 (71)	1.26 (19)	2.0 (12)
7	0.37	43 (82)	0.89 (6)	1.9 (12)

[a] Data for **Sa** and **Sd** in methanol solution. Data for **Sa-AT** and **1**−**7** in aqueous solution (standard buffer). [b] Quantum yield data for **1**−**7** determined using 355 nm excitation by comparison of the peak intensity with that for **Sa-AT**. Estimated error ±10%. [c] Decays and amplitudes for **Sa-AT** and **1**−**7** determined from triple exponential fits of the 390 nm fluorescence decay obtained using 350 nm excitation. [d] Data from ref 24. [e] Data from ref 25. [f] Data from transient absorption measurements. [g] The third component (τ_3 = 12.7 ns) is not considered to be significant.

AT stilbene band extends to a slightly longer wavelength than that of **Sd-AT** as a consequence of extended conjugation provided by the amide groups. The long-wavelength band of **6** and the other donor−acceptor hairpins appears as the sum of the **Sa** and **Sd** absorption bands. Excitation at 355 nm is absorbed predominantly by **Sa**, whereas excitation at 333 nm is absorbed comparably by **Sa** and **Sd**.

The fluorescence properties of **Sa** and **Sd** in methanol have been reported.[24,25] They have emission maxima at 386 and 374 nm, respectively, and fluorescence quantum yields of 0.11 and 0.32 in methanol. Their fluorescence decays are single exponential with decay times of 0.28 and 0.35 ns, respectively. **Sa-An** is nonfluorescent in methanol. The fluorescence maximum for **Sa-AT** is at 389 nm, and its fluorescence quantum yield is 0.38.[3] A fluorescence decay time of 2.0 ns was determined using a stroboscopic instrument with a time resolution of ca. 0.2 ns. **Sd-AT** is nonfluorescent in aqueous solution ($\Phi_f < 10^{-5}$).[25]

The fluorescence spectra of **1**−**7** have band shapes identical to that of **Sa-AT**, which are independent of the excitation wavelength (333 or 355 nm), in accord with the absence of fluorescence from **Sd-AT**. Fluorescence quantum yields were determined by comparison of the peak intensity obtained with 355 nm excitation to that for **Sa-AT**. Values of Φ_f reported in Table 1 increase as the separation between **Sa** and **Sd** increases.

Picosecond Time-Resolved Fluorescence. Fluorescence decays for **Sa-AT** and **2**−**7** were determined using a Ti−Sp based laser system having a time resolution of ca. 35 ps. A sample fluorescence decay for **3** is shown in the Supporting Information (Figure S1) with fits to double and triple exponential functions. Superior fits were achieved with triple exponential functions, particularly in the short time domain (<2 ns). Decay times and amplitudes obtained from triple exponential fits are summarized in Table 1. In all cases, the decays are dominated by short-lived components having decay times of 38−95 ps and amplitudes of 71−82%. The long-lived components for **Sa-AT** and **5**−**7** are similar to those previously determined with 0.2 ns instrument resolution for **Sa-AT** and for other **Sa**-linked hairpins having poly(T:A) base pairs domains with four or more T:A base pairs adjacent to **Sa**.[3] Fluorescence decays were not determined for **Sa-An**, **Sd-AT**, and **1**, all of which are essentially nonfluorescent.

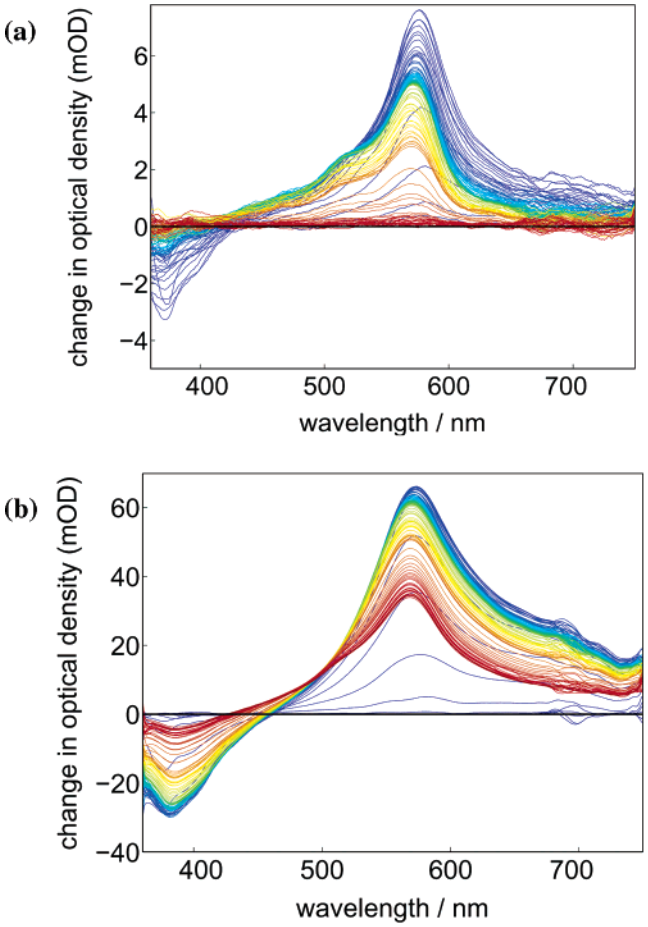

Figure 2. Temporal evolution of the pump−probe spectra of (a) **Sa-An** and (b) **Sa-AT** in the time range of −0.1 ps to 150 ps after excitation at 333 nm. Early spectra are shown in blue/green, and late spectra are shown in orange/red colors.

Femtosecond Pump−Probe Experiments: Reference Compounds. Femtosecond time-resolved transient absorption spectra with a spectral range of 450−750 nm have previously been reported for **Sa**, **Sd**, **Sa-An**, **Sa-AT**, and **Sd-AT**.[3,25] We have repeated these measurements using a Ti−Sp based system with a white-light continuum, which provides a usable probe source between 350 and 750 nm with a time resolution of ca. 150 fs and a spectral resolution of ca. 10 nm.[13] The temporal evolution of the 350−750 nm pump−probe spectra of **Sa** and **Sd** obtained with 333 nm excitation and kinetic analysis of the 570 nm decay is provided as Supporting Information (Figure S2). In agreement with previous studies, their spectra display broad maxima at ca. 575 nm, which rise within ca. 3 ps, and decay components of 362 and 379 ps, respectively, similar to their fluorescence decay times (Table 1). The spectra of both **Sa** and **Sd** also display negative bands at 380 and 360 nm, respectively (Figure S2), which were not observed in previous studies using a narrower spectra detection range. These bands have minima near the fluorescence maxima of **Sa** and **Sd** and are assigned to stimulated emission from their singlet excited states. The decay times of these bands are similar to those of the 575 nm bands.

The temporal evolution of the 350−750 nm pump−probe spectra of **Sa-An** and **Sa-AT** obtained with excitation at 333 nm is shown in Figure 2. Both spectra display rapid growth

(24) Lewis, F. D.; Wu, T.; Burch, E. L.; Bassani, D. M.; Yang, J.-S.; Schneider, S.; Jaeger, W.; Letsinger, R. L. *J. Am. Chem. Soc.* **1995**, *117*, 8785−8792.
(25) Lewis, F. D.; Liu, X.; Miller, S. E.; Hayes, R. T.; Wasielewski, M. R. *J. Am. Chem. Soc.* **2002**, *124*, 11280−11281.

Table 2. Femtosecond Pump−Probe Transient Data[a]

conjugate	380 nm t, ps[b]	575 nm τ, ps[c]	525 nm τ, ps[d]	525/575, ps[e]
Sa-AT	23 (−19) 470 (−5)	18 (25)[f] 790 (32)[g] >2 ns (8.4)[g]	930 (17)[g] >2 ns (3.8)[g]	30
Sd-ATh		0.6[f] 35[g]	32[g]	
1	2.2 (−3.5)	1.5 (6.0)[f] 9.3 (5.8)[g] 490 (1.9)[g]	∼1.0 (−3.8)[f] 9.9 (9.8)[g] 360 (4.2)[g]	1.7
2	25 (−3.4)	24 (3.4)[f] >1 ns (7.6)[g]	31 (−5.1)[f] >1 ns (11)[g]	36
3	53 (−0.57)	33 (1.1)[f] >1 ns (1.3)[g]	41 (1.5)[i] 440 (−1.0)[f] >1 ns (1.8)[g]	290
4	77 (−1.1)	56 (2.4)[f] >1 ns (2.7)[g]	43 (2.7)[i] >1 ns (1.7)[g]	∼1 ns

[a] Rise and decay times (preexponentials in parentheses are negative for components with increasing optical density and positive for components with decreasing optical density). [b] Decay times for the stimulated emission of **Sa***. [c] Decay times for the transient absorption of **Sa*** or **Sd*** (shortest decay times) and $\mathbf{Sa}^{-\bullet}$ (longer decay times). [d] Rise and decay times for the transient absorption of $\mathbf{Sd}^{+\bullet}$ and/or $\mathbf{Sa}^{-\bullet}$. [e] Rise time for the 525/575 nm band intensity ratio attributed to hole injection for **Sa-AT** and hole arrival for **1**−**4**. [f] Component attributed to hole injection or hole arrival. [g] Component attributed to charge recombination. [h] Data from ref 25. [i] Component attributed to charge recombination of $\mathbf{Sd}^{+\bullet}/\mathbf{T}^{-\bullet}$.

(ca. 1 ps) of the 575 and 380 nm transients assigned to the **Sa*** singlet state. In the case of **Sa-An**, the 380 band and the long-wavelength tail of the 575 nm band decay within a few picoseconds accompanied by the rise in the 525 nm shoulder (Figure 2a). The 525/575 nm band intensity ratio also reaches a maximum value of ca. 1:3 within a few picoseconds, and both bands decay with a decay time of ca. 20 ps. These changes have been attributed to charge separation with formation of the $\mathbf{Sa}^{-\bullet}\mathbf{An}^{+\bullet}$ radical ion pair followed by charge recombination.[3] Because the $\mathbf{An}^{+\bullet}$ radical cation does not have an absorption band in this spectral region, both the 575 nm band and the 525 nm shoulder are attributed to $\mathbf{Sa}^{-\bullet}$. Thus, the growth of the 525/575 nm band intensity ratio provides a direct measurement of the charge separation time constant.

The spectral changes observed for **Sa-AT** (Figure 2b) are similar to those observed for **Sa-An**; however, they occur on a much longer time scale. Decay of the negative 380 nm and positive 575 nm bands has fast and slow picosecond components, which are reported in Table 2. The growth of the 525 nm shoulder occurs during the initial phase of the 380 and 575 nm decay. The 525 and 575 nm bands attain a constant band intensity ratio of ca. 1:3 with a rise time of 30 ps and decay together with both a 0.8−0.9 ns component (similar to the slow component of 380 nm decay) and a component that is longer than the experimental 1.9 ns time window. The 380 nm band is outside the spectral window employed in previous studies of **Sa-AT**, and the growth of the 525 nm shoulder was not observed previously.[3] The femtosecond transient spectra of **Sd-AT** have been reported, and the results have subsequently been confirmed.[25] The 575 nm band assigned to **Sd*** decays with a time constant of <0.5 ps concomitant with the growth of the 525 nm band assigned to $\mathbf{Sd}^{+\bullet}$. The 525 nm band has a decay time of 32 ps assigned to charge recombination. Transient decay data for **Sa-AT** and **Sd-AT** are summarized in Table 2.

Femtosecond Pump−Probe Experiments: Donor−Acceptor Hairpins. Pump−probe spectra for **1**−**4** were obtained using 333 nm excitation, the excitation wavelength used for the reference compounds. Both **Sa** and **Sd** absorb at this wavelength (Figure 1). However, because **Sd-AT** is nonfluorescent and rapidly forms a short-lived 525 nm band (Table 2), it is possible to dissect the transient components arising from excitation of **Sa** and **Sd**. Simplification of the spectra at short delay times can be accomplished by excitation of the red-edge of the steady-state absorption spectra, where **Sa** absorbs more strongly than **Sd**. Pump−probe spectra in the time range 0.1−150 ps for hairpins **1**−**4** obtained using 355 nm excitation for **1** and **2** and 333 nm excitation for **3** and **4** are shown in Figure 3 (333 nm excitation data for **1** and **2** are not shown). In all cases, there is an ultrafast rise (<1 ps) of the 575 nm band attributed to **Sa*** and **Sd*** transient absorption and a negative band at 380 nm attributed to **Sa*** stimulated emission (**Sd-AT** is nonfluorescent). In the cases of **2**−**4**, this rise is followed by a fast decay of the 380 and 575 nm bands (ca. 1 ps) attributed to relaxation of the singlet excited states. Spectra for **2**−**4** in the 0.2−1.9 ns time range are shown in Figure S3. Kinetic analysis of the femtosecond pump−probe data for **1**−**4** is presented below and summarized in Table 2, with assignments provided in the footnotes. Negative amplitudes are reported for components with increasing optical density, and positive amplitudes are reported for components with decreasing optical density. The kinetic data extracted from the transient spectra obtained with 333 nm excitation of **1** and **2** (data not shown) are similar to those for 355 nm excitation.

In the case of **1**, the decay of the 380 nm band and the initial decay of the 575 nm band occur with time constants of ca. 2 ps, attributed to charge separation (see Discussion). There is also a fast rising component of the 525 nm transient that is not well resolved from the subsequent fast decay. The rise of the 525/575 nm band ratio (Figure 4) has a time constant of 1.7 ps and is thought to provide the most accurate measure of the time required for charge separation (hole arrival on **Sd**). This ratio attains a maximum value of ca. 2.2:1, substantially larger than the value of ca. 0.3:1 observed for **Sa-TA**. A ratio of 2:1 would be expected for overlapping $\mathbf{Sa}^{-\bullet}$ (1:3) and $\mathbf{Sd}^{+\bullet}$ (525 nm only) transients, assuming that both radical ions have similar molar absorbance. The 525 and 575 nm bands decay with time constants of ca. 9 ps and 0.4 ns, tentatively attributed to charge recombination of the charge separated state prior to and following solvent and nuclear relaxation, respectively.

The spectral changes observed for **2** are similar; however, the time constants are slower. Following the fast relaxation processes that occur within a few picoseconds, the decay of the 380 nm band, the initial decay of the 575 nm band, the rise of the 525 nm band, and the rise of the 525/575 nm band intensity ratio (Figure 4) occur with time constants of 24−36 ps. The decay of the 525 and 575 nm bands is incomplete after 1.9 ns (Figure S3), the longest pump−probe delay time, indicative of slow charge recombination.

Changes in the pump−probe spectra of **3** and **4** (Figure 3) occur more slowly than is the case for **1** or **2**. Following the fast relaxation processes that occur within 1−2 ps, the 380 and 575 nm bands have decay times of 33−77 ps assigned to hole injection, by analogy to the behavior of **Sa-AT**. The 525 nm bands of **3** and **4** have decay times of 41 and 43 ps, attributed to charge recombination of the $\mathbf{Sd}^{+\bullet}/\mathbf{T}^{-\bullet}$ contact radical ion pair by analogy to the behavior of **Sd-AT** (Table 2).[25] The 41 ps decay for **3** is followed by a slow rise with time constant of

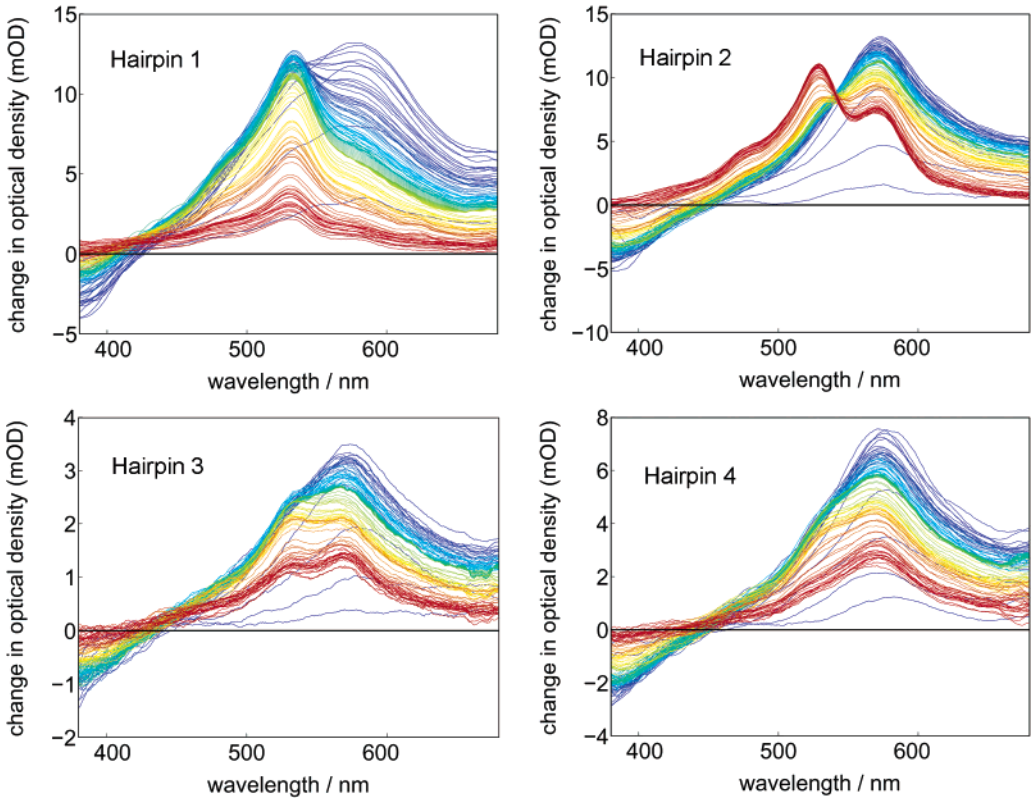

Figure 3. Temporal evolution of the pump−probe spectra of hairpins **1**−**4** in the time range of −0.1 ps to 150 ps after excitation at 355 nm (**1** and **2**) or 333 nm (**3** and **4**). Early spectra are shown in blue/green, and late spectra are shown in orange/red colors.

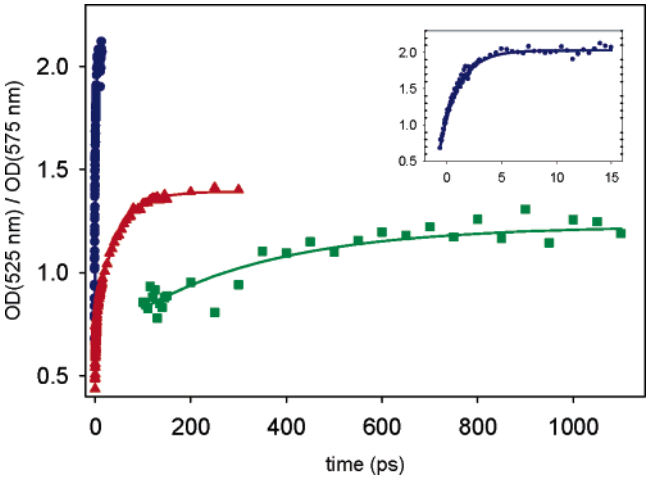

Figure 4. Time dependence of the 525/575 nm band intensity ratios for **1** (inset), **2** (Δ), and **3** (□).

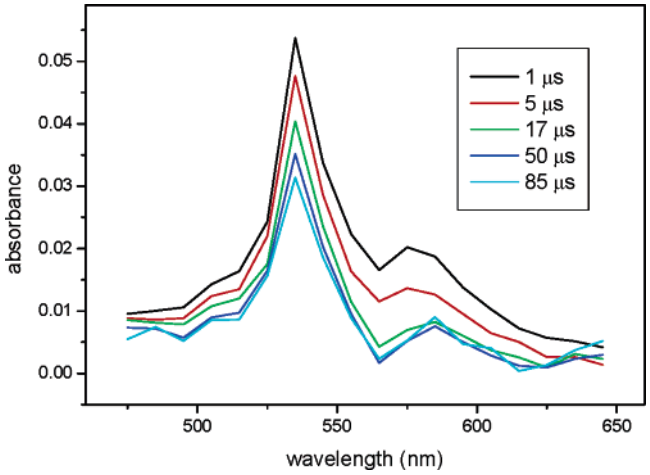

Figure 5. Nanosecond time-resolved spectra of **6**. The 525 nm band is assigned to overlapping absorption of $\mathbf{Sd}^{+\bullet}$ and $\mathbf{Sa}^{-\bullet}$, and the 575 nm band is assigned to absorption of $\mathbf{Sa}^{-\bullet}$.

0.44 ns. Similarly, the 525/575 nm band intensity ratios display an initial decrease (due to the fast decay of the 525 nm band created by direct excitation of **Sd**) followed by a rise with a time constant of 0.29 ns for **3** (Figure 4) and ca. 1 ns for **4** (Figure S3), attributed to hole arrival. Decay of the 525 and 575 nm bands of **3** and **4** is incomplete after 1.9 ns (Figure S3), indicative of slow charge recombination.

Nanosecond Transient Absorption. The transient absorption spectra of **3**−**7** were obtained using 355 nm excitation provided by nanosecond Nd:YAG laser pulses and a pulsed xenon arc lamp for detection with an instrument response time of ca. 30 ns.[14] Satisfactory signal/noise ratios were observed after a single laser pulse for argon-purged solutions and are independent of the number of laser pulses, even though sample degradation occurs with repeated pulsing. Sample degradation occurs rapidly in the presence of oxygen. The time-resolved spectra for conjugate **6** are shown in Figure 5. As is the case for the femtosecond transient spectra, the absorption band at 525 nm is assigned to overlapping absorption of $\mathbf{Sd}^{+\bullet}$ and $\mathbf{Sa}^{-\bullet}$ and the band at 575 nm is assigned to $\mathbf{Sa}^{-\bullet}$. Similar spectra were obtained for the other donor−acceptor hairpins. The rise times for these spectra were not resolved and thus are assumed to be comparable to or faster than the instrument response time. Decay traces obtained at 525 and 575 nm are best fitted by single-exponential functions, which are assigned to charge recombination (Table 3). Similar decay times were obtained at both

Table 3. Nanosecond Laser Flash Photolysis Transient Decays[a]

conjugate	575 nm, μs	525 nm, μs
2	0.0084[b]	
3	0.22	0.23
4	8.5	8.4
5	30	30
6	160	140
7	590	830

[a] Single-exponential fits to the transient decays. [b] Data from ref 15.

Chart 2. Singlet Energies and Reduction Potentials of Several Arenedicarboxamides[26]

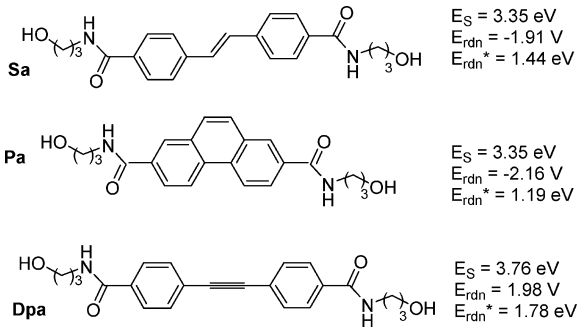

wavelengths, except in the case of **7**, which has the weakest transient signals. In the case of **Sa-AT**, a weak 575 nm transient signal with a decay time of 290 ns was observed, whereas no long-lived transient could be observed for **Sd-AT**.

Discussion

Our approach to the study of the distance and driving force dependence of DNA electron-transfer dynamics has employed synthetic DNA hairpins in which an organic chromophore serves both as the hairpin linker and as a singlet state electron acceptor.[26] The distance-dependent dynamics of DNA electron transfer were initially investigated in hairpins possessing the **Sa** linker (e.g., **Sa-AT**, Chart 1) and a single G:C base pair separated by a variable number of A:T base pairs.[2,3] The free energy for electron transfer from G to **Sa*** was estimated to be ca. -0.20 eV, using Weller's equation ($\Delta G_{et} = -E_S - E_{rdn} + E_{ox}$), the measured singlet energy and oxidation potential of **Sa** (Chart 2), and the reported oxidation potential of G (1.24 V vs SCE in acetonitrile).[27,28] Rate constants for charge separation and charge recombination in **Sa/G** systems were obtained from analysis of the femtosecond transients assigned to the decay of **Sa*** and $\mathbf{Sa}^{-\bullet}$. The formation and decay of $\mathbf{G}^{+\bullet}$ is not directly observed due to the absence of measurable transient absorption. Analysis of the kinetic data for **Sa/G** hairpins using a superexchange model provided a distance dependence of $\beta = 0.65$ Å^{-1} for charge separation and $\beta = 0.95$ Å^{-1} for charge recombination.[2]

Donor−acceptor capped hairpin systems related to **2**−**7** were introduced several years ago for the study of DNA electron-transfer dynamics and exciton-coupled circular dichroism.[15,29] The lower oxidation potential of **Sd** ($E_{ox} = 0.92$ V vs SCE) versus G results in more exergonic photoinduced electron transfer ($\Delta G_{et} = -0.52$ eV) than the value estimated with G as the electron donor. The well-resolved transient absorption spectra of the $\mathbf{Sa}^{-\bullet}/\mathbf{Sd}^{+\bullet}$ charge-separated state provide definitive evidence for the occurrence of charge separation and charge recombination via a DNA bridge. The values of β for charge separation and charge recombination in these systems are similar to those for the **Sa/G** hairpin systems.[15] However, in the published transient data neither the **Sa/G** nor the **Sa/Sd** system serves to distinguish between a single-step superexchange process (Scheme 1a) and a multistep hopping process, in which the distance-dependent time constant for charge separation would, in effect, become the hole arrival time on guanine (Scheme 1b).

In view of the continuing uncertainty about the mechanism and dynamics of charge separation and charge migration processes in DNA, we have undertaken a comprehensive study of the **Sa/Sd** capped hairpin systems **1**−**7** shown in Chart 1. These capped hairpins have simpler structures than the capped hairpins studied previously, which possess 5′-nucleotides.[15,29] The present studies provide (a) a wider spectral range for femtosecond pump−probe measurements, (b) improved time resolution for fluorescence decay measurements, and (c) nanosecond transient absorption measurements for capped hairpins with longer base pair domains.

Linkers and Hairpins. The photochemical behavior of the stilbene linkers **Sa** and **Sd** has been well characterized.[3,25] The singlet states of both stilbenes display strong fluorescence and transient absorption (Figure S2) with decay times of 280−380 ps (Table 1). Extension of the transient spectral measurements to include the 350−450 nm spectral region permits observation of the stilbene stimulated emission, which has the same decay time as the fluorescence and transient absorption.

As in our previous studies, the covalently linked donor−acceptor **Sa-An** serves as a model for conversion of the **Sa*** singlet state to the anion radical $\mathbf{Sa}^{-\bullet}$.[3] Its pump−probe spectra in methanol (Figure 2a) display growth of the **Sa*** 575 nm transient absorption and 380 nm stimulated emission within the first picoseconds, followed by rapid decay of the 380 nm band and of the red-edge of the 575 nm band, as well as growth of the 525 nm shoulder, with time constants of ca. 1.0 ps. The resultant spectrum is assigned to $\mathbf{Sa}^{-\bullet}$. It has a 525/575 nm band intensity ratio of ca. 1:3 and a decay time of ca. 20 ps. The rise and decay times are faster than those previously determined in tetrahydrofuran solvent,[3] in accord with the known effect of solvent polarity on the dynamics of charge separation and charge recombination in donor−acceptor systems with flexible tethers.[30]

In our previous studies of **Sa-AT**, the high fluorescence quantum yield, long fluorescence decay time, and absence of pronounced changes in the transient absorption band shape were taken as evidence for the absence of photoinduced charge separation.[3] The femtosecond pump−probe spectra of **Sa-AT** (Figure 2b) reveal both a fast decay of the stimulated emission of **Sa*** and a rise of the 525/575 nm band intensity ratio, similar to the changes observed for **Sa-An** (Figure 2a). These processes have time constants of 20−30 ps. Reinvestigation of the

(26) (a) Lewis, F. D.; Letsinger, R. L.; Wasielewski, M. R. *Acc. Chem. Res.* **2001**, *34*, 159−170. (b) Lewis, F. D.; Wu, Y. *J. Photochem. Photobiol., C: Rev.* **2001**, *2*, 1−16. (c) Lewis, F. D.; Wasielewski, M. R. In *Charge Transfer in DNA*; Wagenknecht, H. A., Ed.; Wiley-VCH: Weinheim, 2005; pp 93−116.
(27) Weller, A. *Z. Phys. Chem. Neue. Folg.* **1982**, *133*, 93−98.
(28) Seidel, C. A. M.; Schulz, A.; Sauer, M. H. M. *J. Phys. Chem.* **1996**, *100*, 5541−5553.
(29) Lewis, F. D.; Wu, Y.; Hayes, R. T.; Wasielewski, M. R. *Angew. Chem., Int. Ed.* **2002**, *41*, 3485−3487.
(30) (a) Mataga, N.; Nishikawa, S.; Asahi, T.; Okada, T. *J. Phys. Chem.* **1990**, *94*, 1443−1447. (b) Okada, T.; Migita, M.; Mataga, N.; Sakata, Y.; Misumi, S. *J. Am. Chem. Soc.* **1981**, *103*, 4715−4720.

Table 4. Summary of Kinetic Data for Hole Arrival, Hole Injection, and Charge Recombination

conjugate	hole injection 10^{-10} k_i, s^{-1} [a]	hole arrival 10^{-10} k_a, s^{-1} [b]	charge recombination 10^{-8} k_t, s^{-1} [c]
Sa-AT	3.3[b]		
1		58	24
2	2.6 (4.0)	2.7	1.2
3	1.5 (1.9)	0.34	4.4×10^{-2}
4	2.5 (1.3)	0.1	1.2×10^{-3}
5	1.2		3.3×10^{-4}
6	1.1		6.7×10^{-5}
7	2.3		1.4×10^{-5}

[a] Estimated from the fast component of fluorescence decay (Table 1) or from the decay of the 380 nm stimulated emission (Table 2, data in parentheses). [b] Estimated from the rise in the 525/575 nm band intensity ratio (Table 2). [c] Estimated from the average of the 525 and 575 nm transient decays (Tables 2 and 3).

fluorescence properties of **Sa-AT** with picosecond time resolution reveals a major fluorescence decay component having a decay time of 45 ps, near the time resolution of the picosecond fluorescence instrument (Table 1). Both the decay of the fluorescence and the 575 nm femtosecond transient absorption of **Sa-AT** display longer lived components with decay times of 0.5−2.0 ns (Tables 1 and 2).

On the basis of these observations, the fast decay of **Sa*** and formation of $\mathbf{Sa}^{-\bullet}$ in **Sa-AT** are attributed to hole injection to the poly(A:T) base pair domain, which occurs with a rate constant of $k_i \approx 3 \times 10^{10}$ s^{-1} (Table 4), significantly slower than the rate constant of 1×10^{12} s^{-1} previously reported for oxidation of a neighboring guanine by **Sa***.[31] The longer lived 0.86 and 2.2 ns fluorescence decay components (Table 1) and similar transient decays (Table 2) for **Sa-AT** are attributed to charge recombination processes for charge separated states with one or more A:T base pairs separating the radical ions. Charge recombination to regenerate the fluorescence singlet state is commonly observed for singlet contact radical ion pairs and donor−bridge−acceptor charge separated states.[32] Alternatively, the longer lived fluorescence decays might be attributed to multiple hairpin conformations with different lifetimes, as has been suggested for aminopurine fluorescence decay in DNA duplex structures.[5,33] However, molecular dynamics simulations for **Sa**-capped hairpins indicate that they are conformationally homogeneous.[22] Furthermore, the similarity of the fluorescence and 575 nm transient decay times for **Sa-AT** suggests that the decay of **Sa*** and of $\mathbf{Sa}^{-\bullet}$ are related processes, in accord with the occurrence of reversible hole injection.

Charge Separation in Donor−Acceptor Hairpins. The observation of reversible hole injection for **Sa-AT** suggests that charge separation in the donor−acceptor hairpins **1**−**7** might occur via either a hopping mechanism or the previously proposed superexchange mechanism. As discussed in the Results, the rise time of the 525/575 nm band intensity ratio provides the time required for arrival of a hole on **Sd**, which is

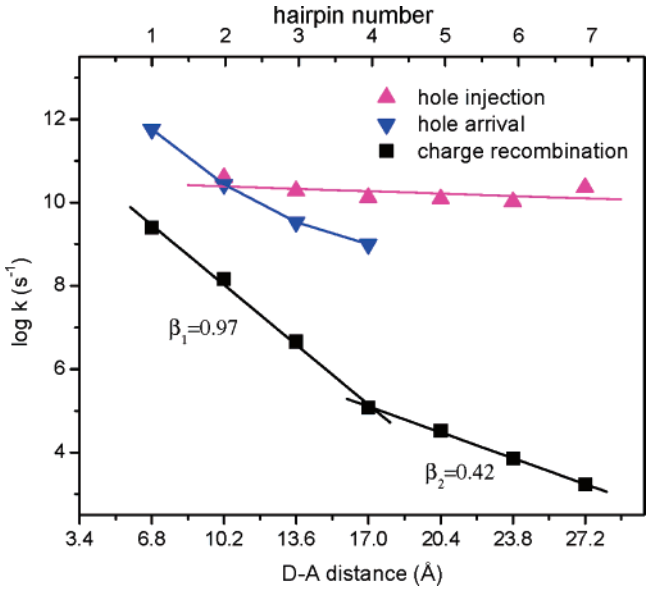

Figure 6. Distance dependence of the rate constants for hole injection, hole arrival, and charge recombination.

independent of the charge separation mechanism. Rate constants for hole arrival, k_a, for **1**−**4** obtained from femtosecond pump−probe data (Figures 3 and 4) are summarized in Table 4 and in Figure 6. Hole arrival rates for **5**−**7** are too slow for study with our femtosecond apparatus and too fast for our nanosecond apparatus. Based on the time resolution of these experiments, values of 5×10^8 $s^{-1} > k_a > 5 \times 10^7$ s^{-1} can be estimated for **5**−**7**. The plot of k_a versus R_{DA} shown in Figure 6 displays curvature, indicative of a possible change in mechanism. However, the slope obtained from a linear fit to the data for **1**−**4** provides a value of $\beta = 0.67$ $Å^{-1}$, essentially the same as that reported previously for charge separation in **Sa/G** hairpin systems ($\beta = 0.65$ $Å^{-1}$).[2]

The **Sa*** decay times for **1**−**4** can be obtained from the decay of the 380 nm stimulated emission (Table 2), and the decay times for **2**−**7** can be obtained from the fluorescence decays (Table 1). In the case of **1**, the decay time of the 380 nm stimulated emission is similar to the rise of the 525/575 nm band ratio, both of which are significantly faster than the hole injection time for **Sa-AT**. These data are consistent with a single-step superexchange mechanism for charge separation. The assignment of transients and the kinetic behavior of **1** are summarized in Scheme 2a. It is possible that the behavior of **1** is influenced by nondegenerate exciton coupling between the two stilbenes. A 5 nm red-shift in the absorption maximum is observed for a capped hairpin possessing two **Sa** chromophores separated by a single base pair, in agreement with a calculated exciton splitting of 560 cm^{-1}.[22] However, there is no detectable shift in the absorption or fluorescence spectra of **1** when compared to **2**−**7**.

In the case of both **3** and **4**, the fast components of the fluorescence decays (Table 1) and the 380 nm transient decays (Table 2) are distinctly faster than their hole arrival times (Table 4). The assignment of transients and the kinetic behavior of **3** are summarized in Scheme 2b. Values of k_i for **3**−**7** estimated from the fluorescence and 380 nm transient decays are reported in Table 4. Hole arrival times are not available for **5**−**7**; however, they presumably are slower than the hole injection rates provided by the fast component of fluorescence decay.

(31) Lewis, F. D.; Kalgutkar, R. S.; Wu, Y.; Liu, X.; Liu, J.; Hayes, R. T.; Wasielewski, M. R. *J. Am. Chem. Soc.* **2000**, *122*, 12346−12351.
(32) (a) Gould, I. R.; Farid, S. *Acc. Chem. Res.* **1996**, *29*, 522−528. (b) Overing, H.; Paddon-Row, M. N.; Heppener, M.; Oliver, A. M.; Cotsaris, E.; Verhoeven, J. W.; Hush, N. S. *J. Am. Chem. Soc.* **1987**, *109*, 3258−3269. (c) Gould, I. R.; Young, R. H.; Mueller, A.; Albrecht, A. C.; Farid, S. *J. Am. Chem. Soc.* **1994**, *116*, 8188−8199. (d) Lor, M.; Thielemans, J.; Viaene, L.; Cotlet, M.; Hofkens, J.; Weil, T.; Hampel, C.; Muellen, K.; Verhoeven, J. W.; Van der Auweraer, M.; De Schryver, F. C. *J. Am. Chem. Soc.* **2002**, *124*, 9918−9925.
(33) Rachofsky, E. L.; Osman, R.; Ross, J. B. A. *Biochemistry* **2001**, *40*, 946−956.

Scheme 2. Dynamics of Charge Separation and Charge Recombination in (a) Hairpin **1** and (b) Hairpin **3** (Hole on Bridge Shown As Being Localized on the Middle A)[a]

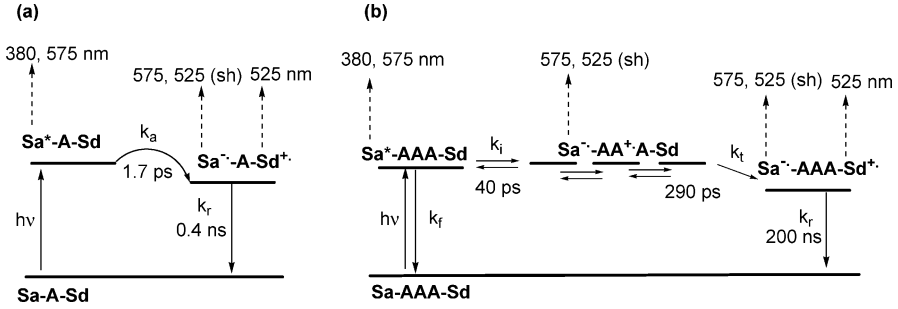

[a] Dashed arrows indicate transient assignments.

Thus, we conclude that charge separation in conjugates **3**−**7** occurs via a multistep mechanism consisting of photoinduced hole injection (k_i), followed by hole transport (A-hopping) and hole trapping by **Sd** (k_t, Scheme 2b).

The kinetic behavior of **2** is intermediate between that of **1** and **3**. As is the case for **1**, the decay of **Sa*** (Table 1) and the rise of the 525/575 nm band ratio (Table 2) have similar time constants. The hole arrival rate for **2** is similar to the hole injection rate for **Sa-AT**, **3**, and **4**. These data are consistent with either a superexchange mechanism or a hopping mechanism, in which hole injection is slower than hole trapping and thus rate determining. If we assume a value of $\beta \approx 1.0$ Å^{-1} for superexchange, similar to that for charge recombination (see below), the rate constant for hole arrival in **2** would be ca. 3×10^9 s^{-1}. This value is smaller than either the value of k_a determined from the rise of the 525/575 nm absorption band ratio or the value of k_i estimated from either the fluorescence decay or the decay of the 380 nm transient (Table 2). Thus, we tentatively conclude that charge separation in **2** occurs via a hopping mechanism.

Hole Injection and Hole Transport. The observation of both short-lived and long-lived components for the decay of the **Sa*** fluorescence and stimulated emission in **Sa-AT** indicates that the hole injection process is reversible. As such, these decay components cannot be assigned to individual kinetic processes by means of simple first-order analysis. The fast 40−90 ps fluorescence decay components presumably represent the reversible formation of a $\mathbf{Sa}^{-\bullet}/\mathbf{A}^{+\bullet}$ contact radical ion pair, whereas the longer lived components may arise from the charge recombination of $\mathbf{Sa}^{-\bullet}/\mathbf{A}^{+\bullet}$ radical ion pairs separated by one or more A:T base pairs. The short-lived fluorescence decay times are independent of the length of the A-tract in **2**−**7** and are significantly slower than the 1 ps hole injection time for the **Sa*/G** system. Based on our studies of the driving force dependence of hole injection to an adjacent nucleobase in DNA hairpins, a **Sa*** decay time of ca. 50 ps is indicative of a value of $\Delta G_i \approx 0$ eV.[31] Comparison to the value of $\Delta G_i = -0.2$ eV for photooxidation of G suggests that the difference in oxidation potentials for G versus A is ca. 0.2 eV, smaller than earlier estimates based on nonaqueous oxidation potentials.[28] However, this value is entirely consistent with estimates from time-resolved charge-transfer dynamics in bimolecular nucleotide complexes and with studies of hole transport dynamics and equilibria.[34,35]

In principle, the dynamics of the individual steps in the reversible hole injection and hole migration processes might be determined from the decay times and preexponentials for the decay of **Sa*** and/or from the hole arrival times. However, because the fast fluorescence decay components are near the time resolution of our instrumentation, fluorescence data with improved time resolution as well as hole arrival times from nanosecond pump−probe experiments for hairpins **2**−**7** would be required for complete kinetic analysis of the reversible hole injection and hole migration processes. Takada et al. have estimated a value of 2×10^{10} s^{-1} for the rate constant for A-hopping from an analysis of the distance dependence of the quantum yields for charge separation in systems having a naphthaldiimide acceptor and phenothiazine donor, assuming a random walk mechanism.[36,37]

The efficiency of charge separation for **2**−**7** has not been determined directly. However, the modest decrease in the pump−probe spectral intensity for **3** and **4** at long delay times (Figure S3) and the observation of the charge separated state with a single nanosecond laser pulse (Figure 5) are indicative of efficient charge separation. The fluorescence quantum yields of $\Phi_f \approx 0.3$ for **4**−**6** (Table 1) place an upper bound of Φ_{cs} for the charge separation efficiencies ($\Phi_{cs} \leq 1 - \Phi_f$).

Charge Recombination. The observation of similar first-order rate constants for decay of both the $\mathbf{Sd}^{+\bullet}$ and the $\mathbf{Sa}^{-\bullet}$ transient absorption bands (Figures 3 and 5) provides definitive evidence for decay of the charge separated state via charge recombination. Rate constants for charge recombination are summarized in Table 4, and their distance dependence is shown in Figure 6. The longer time constant for charge recombination versus charge separation in **1** (Scheme 2a) is consistent with the large energy gap for charge recombination, which is responsible for Marcus inverted kinetics.[31] The values for k_{cr} decrease from 1.0×10^{11} s^{-1} for **1** to 1.4×10^3 s^{-1} for **7**, a dynamic range of nearly 10^8! The values of k_r for **1**−**4** provide a value of $\beta = 0.97$ Å^{-1}, similar to that reported for **Sa/G** systems.[3] The values of k_r for **5**−**7** display a weaker distance dependence with a value of $\beta = 0.42$ Å^{-1}.

The values of $\beta \approx 1.0$ Å^{-1} for charge recombination in **1**−**4** and **Sa/G** systems are similar to that for charge separation in donor−bridge−acceptor systems with protein β-strand bridges, which undergo electron transfer via a single-step superexchange

(34) Lewis, F. D.; Wasielewski, M. R. *Top. Curr. Chem.* **2004**, *236*, 45−65.
(35) Fiebig, T.; Wan, C.; Zewail, A. H. *ChemPhysChem* **2002**, *3*, 781−788.
(36) Takada, T.; Kawai, K.; Cai, X.; Sugimoto, A.; Fujitsuka, M.; Majima, T. *J. Am. Chem. Soc.* **2004**, *126*, 1125−1129.
(37) Kawai, K.; Takada, T.; Tojo, S.; Fujitsuka, M.; Majima, T. *J. Am. Chem. Soc.* **2003**, *125*, 6842−6843.

mechanism.[38] The value of $\beta \approx 0.4$ Å^{-1} for charge recombination in **5**−**7** is similar to the values reported by Shafirovich et al.[39] for hole transport from aminopurine cation radical to guanine and by Takada et al. for naphthaldiimide/phenothiazine systems separated by 4−8 A:T base pairs.[36] The smaller slope may reflect an increasing contribution of multistep hole hopping to the charge recombination dynamics at longer distances.[40] If so, the onset of crossover occurs at much larger value of R_{DA} (five intervening base pairs or ca. 20 Å) than is the case for charge separation. Abdel Malak et al. have recently reported a crossover in mechanism for electron transfer across helical poly(proline) bridges from superexchange ($\beta = 1.4$ Å^{-1}) to hopping ($\beta = 0.18$ Å^{-1}) that occurs at a donor−acceptor edge-to-edge distance of ca. 20 Å.[8]

The occurrence of crossover from superexchange to hole hopping at a longer distance for charge recombination than for charge separation is a consequence of donor−bridge acceptor energetics. Whereas reversible hole injection is approximately isoergonic, hole trapping by **Sd** is estimated to be exergonic by ca. 0.5 eV (Scheme 2a). Paulson et al. have recently reported that rate constants for superexchange are only weekly dependent upon the free energy for electron transfer, whereas rate constants for hopping are strongly dependent upon the free energy change.[9] Thus, superexchange will dominate at short distances when ΔG_{et} is large, as it is for charge recombination in **2**−**4**.

Concluding Remarks

The observation of charge separation via a multistep hole hopping mechanism for **Sa/Sd** hairpin systems possessing two or more A:T base pairs necessitates reexamination of the literature relating to the mechanism and dynamics of photoinduced charge separation in donor−bridge−acceptor systems with DNA bridges. The results of collaborative studies in our laboratories indicate that charge separation in **Sa/G** systems with two or more intervening A:T base pairs also occurs via hole hopping rather than superexchange. A hole hopping mechanism can also readily explain the observation of similar rate constants for charge separation in **Sa**-linked hairpins possessing **Sd**, G, GG, GGG, and Z hole traps.[41] Increasing the depth of the hole trap should have little effect on the dynamics of charge separation in these systems. Rate constants reported in our previous study of reversible hole transport between primary and secondary hole traps are not dependent upon the assumed mechanism for hole injection and thus should not require revision.[34]

The use of different singlet acceptors can affect the competition between superexchange versus hole hopping. Hole injection for the weaker phenanthrenedicarboxamide acceptor **Pa** (Chart 2) is estimated to be endergonic by ∼0.25 eV.[39] The distance dependence of singlet quenching of **Pa*** by deazaguanine separated by 1−3 A:T base pairs provides a value of $\beta = 1.1$ Å^{-1}, consistent with a superexchange mechanism, as previously proposed. The singlet acridinium acceptor **Acr*** studied by Fukui and by Michel-Beyerle reportedly does not oxidize neighboring A.[4] Oxidation of G or Z by **Acr*** is strongly distance dependent ($\beta \approx 1.4$ Å^{-1}), consistent with a superexchange mechanism. Values of $\beta > 1$ Å^{-1} have also been reported for DNA-mediated photoinduced charge separation between both intercalated and end-tethered donor−acceptor pairs, which are not capable of hole injection.[42]

Hole injection for the stronger acceptor diphenylacetylene dicarboxamide **Dpa** (Chart 2) is estimated to be exergonic by ∼0.1 eV. Rate constants for conversion of **Dpa** to **Dpa**$^{-\bullet}$ are independent of the presence of guanine, consistent with a hopping mechanism for **Dpa/G** systems with 1−5 intervening A:T base pairs.[43] Reanalysis of the published results for these systems indicates that hole trapping by guanine does occur following hole injection and hole transport. Photoinduced charge separation in systems having an intercalated ethidium acceptor and deazaguanine donor is also reported to occur via hole injection followed by irreversible hole trapping.[5]

The behavior of the **Pa/Z** and **Dpa/G** systems provides examples of superexchange and hopping mechanisms, respectively, whereas the **Sa/Sd** system exhibits crossover between these two limiting mechanisms. Another likely example of crossover is provided by the results of Wan et al. for photoinduced electron transfer in systems possessing an aminopurine (**Ap**) acceptor and guanine donor separated by several A:T base pairs.[6] An increase in **Ap*** lifetime with increasing **Ap/G** separation is attributed to competing superexchange quenching by G and A, but also could result from reversible hole injection followed by distance-dependent charge trapping by G.

In summary, the coordinated application of several transient spectroscopic methods has succeeded in disentangling for the first time the complex kinetics of photoinduced charge separation and charge recombination in DNA. Charge separation is found to occur via a single-step superexchange mechanism only at short donor−acceptor distances. At longer distances, charge separation occurs via a multistep mechanism: hole injection, hole migration, and hole trapping. The superexchange, hole migration, and charge recombination processes are all distance dependent, whereas the hole injection process is independent of donor−acceptor distance, but dependent upon its energetics. The dynamics and mechanism of hole migration in A-tracts and other base sequences are the subjects of continuing investigation.

Acknowledgment. This research is supported by the Office of Basic Energy Sciences, U.S. Department of Energy under Contract DE-FG02-96ER14604 (F.D.L.), Boston College (T.F.), and the National Institutes of Health, Grant 5 R01 ES11589, and the Kresge Foundation (V.S.).

Supporting Information Available: Fluorescence decay traces for **3**, transient absorption spectra for **Sa** and **Sd**, and transient absorption spectra for **2**−**4** at delay times of 0.2−1.9 ns. This material is available free of charge via the Internet at http://pubs.acs.org.

JA0540831

(38) Gray, H. B.; Winkler, J. R. In *Electron Transfer in Chemistry*; Balzani, V., Ed.; Wiley-VCH: Weinheim, 2001; Vol. 3, pp 3−23.
(39) (a) Shafirovich, V. Y.; Dourandin, A.; Huang, W.; Luneva, N. P.; Geacintov, N. E. *Phys. Chem. Chem. Phys.* **2000**, *2*, 4399−4408. (b) Shafirovich, V. Y.; Geacintov, N. E. *Top. Curr. Chem.* **2004**, *237*, 129−157. (c) Shafirovich, V. Y.; Geacintov, N. E. In *Charge Transfer in DNA*; Wagenknecht, H. A., Ed.; Wiley-VCH: Weinheim, 2005; pp 175−196.
(40) Takada, T.; Kawai, K.; Fujitsuka, M.; Majima, T. *Proc. Natl. Acad. Sci. U.S.A.* **2004**, *101*, 14002−14006.
(41) (a) Lewis, F. D.; Liu, X.; Liu, J.; Hayes, R. T.; Wasielewski, M. R. *J. Am. Chem. Soc.* **2000**, *122*, 12037−12038. (b) Lewis, F. D.; Liu, J.; Liu, X.; Zuo, X.; Hayes, R. T.; Wasielewski, M. R. *Angew. Chem., Int. Ed.* **2002**, *41*, 1026−1028.
(42) (a) Harriman, A. *Angew. Chem., Int. Ed.* **1999**, *38*, 945−949. (b) Barbara, P. F.; Olson, E. J. C. *Adv. Chem. Phys.* **1999**, *107*, 647−676. (c) Meade, T. J.; Kayyem, J. F. *Angew. Chem., Int. Ed. Engl.* **1995**, *34*, 352−354.
(43) Lewis, F. D.; Liu, X.; Miller, S. E.; Hayes, R. T.; Wasielewski, M. R. *J. Am. Chem. Soc.* **2002**, *124*, 14020−14026.